1

LCOS Spatial Light Modulators: Trends and Applications

Grigory Lazarev, Andreas Hermerschmidt, Sven Krüger, and Stefan Osten

1.1
Introduction

Spatial light modulator (SLM) is a general term describing devices that are used to modulate amplitude, phase, or polarization of light waves in space and time. Current SLM–based systems use either optical MEMS (microelectromechanical system, [1]) or LCD technology [2]. In this chapter, we review trends and applications of SLMs with focus on liquid crystal on silicon (LCOS) technology.

Most developments of liquid crystal (LC) microdisplays are driven by consumer electronics industry for rear–projection TVs, front projectors, and picoprojectors. Also, MEMS technologies such as digital micromirror device (DMD, [3]) and grating light valve (GLV, [4]) are driven by these industries, except for membrane mirrors. Some industrial applications have forced MEMS development for scanning, printing technologies, and automotive applications [5]. But the major R&D-related driving force for new SLM technologies is the defense industry.

Technological advances in lithography are the basis for MEMS developments. Phase modulators based on 2D pistonlike mirror arrays [6, 7] or ribbonlike 1D gratings [8] show high performance in frame rate. Unfortunately, the availability of these technologies is limited because they are developed either company-internal or within defence projects. The major advantages of MEMS are frame rate, spectral range, and an efficient use of nonpolarized light. Phase modulators and other optical implementations are still niche markets for the MEMS industry. Even now, customized MEMS developments are quite challenging and expensive.

LC panels still have an advantage out of their projection applications in terms of resolution and minimal pixel size for 2D displays. Only LC-based technology is able to modulate intensity, phase, and/or polarization because of polarization rotation and/or electrically controlled birefringence (ECB).

LCOS technology [9] was developed for front- and rear- (RPTV) projection systems competing with AMLCD (active matrix LCD) and DMD. The reflective arrangement due to silicon backplane allows putting a high number of pixels in a small panel, keeping the fill factor ratio high even for micrometer-sized pixels.

The history of companies shutting down their LCOS activities (Intel, Philips, etc.) and the downfall of the RPTV market made it difficult to demonstrate the promised LCOS advantages in performance and volume pricing. However, the classic three-panel architectures for high-end front- and rear-projection systems led to the development of high-quality microdisplays, high-performance polarization, and compensation optics as well as sophisticated electronic driving solutions. Single-panel designs for field sequential color systems never really entered the high-end and professional market, but are as good candidates as DMD and laser scanning technologies for small and embedded projection devices, such as cell phone, companion, camera, and toy projectors.

1.2
LCOS-Based SLMs

LCOS SLMs based on "consumer" microdisplay technology inherited features and drawbacks of projection displays. Backplanes of the front-projection microdisplays usually have a diagonal exceeding 0.55 in. or higher and pixel sizes starting from 8 μm. Smaller panels are not popular in front-projection microdisplays because of étendue limitations when used in an incoherent system [10] as well as heat dissipation considerations. However, microdisplays intended for embedded projectors and picoprojectors utilize quite small panels from 0.17 to 0.55 in. with pixel sizes ranging from 6 to 10 μm. Whereas HMD products require a larger panel diagonal for high field of view (FOV) designs. Reduction of the pixel size has a significant economical advantage in customer electronics industry since it allows placing more dies on the wafer. Both types of microdisplays are usually driven color field sequential, which means they offer a higher frame rate when potentially used as SLMs.

1.2.1
LCOS Technology

1.2.1.1   **Manufacturing and Assembly Technologies**
LCOS technology has different descriptions/brand names with different suppliers; for example, JVC's "D-ILA" and Sony's "SXRD," are basically the same CMOS wafer technology, processed typically using 8 in. silicon wafers (Figure 1.1). Both Sony and JVC introduced 4K LCOS panels (4096 × 2160 and 4096 × 2400) to the market. JVC was also successful in building a prototype of an 8K panel (8192 × 4320) with 5 μm pixel size [11].

In order to get a good reflectivity out of these reflective pixelated arrays, high reflective aluminum mirrors, mostly with a passivation layer, are used. Various techniques for planarization or reduced interpixel gap effects have been developed over the years. At present, foundries offer processes to reduce the interpixel gap in the design down to 200 nm [12].
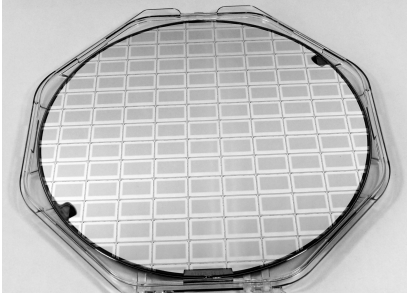
Figure 1.1 Silicon wafer with panel backplanes of Omnivision (OVT).

It is also possible to cover the backplane with a dielectric mirror so that the pixelated structure is not seen any more. It allows to increase the reflectivity of the SLM, so the light utilization efficiency for a low-frequency content is higher. Unfortunately, dielectric layers limit the spectral range of the device typically to an 80–100 nm band. Another disadvantage is that the cell requires higher voltages as it becomes thicker and therefore introduces a higher cross talk between adjacent pixels. As the modulation is then strongly dependent on the addressed spatial frequency, the effective resolution of the microdisplay as well as the achievable diffraction efficiency will decrease. The pixel resolution of such commercially available SLMs (Hamamatsu Photonics, Boulder Nonlinear Systems) does not exceed SVGA, and pixel sizes are typically as large as 16–32 μm [13].

The production of the actual LCOS cell can be done on the wafer level or based on single cell. The LCOS cell production on the wafer level has advantages on the economics side but lacks flexibility. An important process is the implementation of the spacers, defining the cell gap of the LCOS cell. There are spacers designed into the CMOS backplane, spacers distributed into the LC material itself, and also spacers as part of the gasket definition (frame spacer technology). Assembled LCOS cells typically show a dashed shape (Figure 1.2). Wafer-scale-processed parts have a lower curvature than single-cell-assembly-manufactured parts [2].

In the peak of the RPTV and front-projection development phase, the alignment layer technologies became an important factor because of lifetime issues with higher-density illumination and the lower end of the blue spectrum. So, the standard alignment layer material polyimide (PI) was replaced by inorganic SiO_x alignment structures [14]. Besides projection applications various LC modes for photonic applications [15] were also designed and tested, covering twisted nematic, ECB, and VAN (vertically aligned nematic) materials. In order to use the LCOS as an addressable optical component the packaging design and the packaging processes, such as die attach/bonding and wire bonding, as well as device handling are critical. Packaging also significantly influences the total device cost when going into volume production.

Related to HOLOEYE's history in diffractive optics and SLM technologies, we developed phase modulating LCOS SLMs in conjunction with Omnivision Technologies (OVT), see [16]. The phase modulating LCOS SLMs are based on

PV: 3.0
RMS: 0.6
μm

Points: 44902
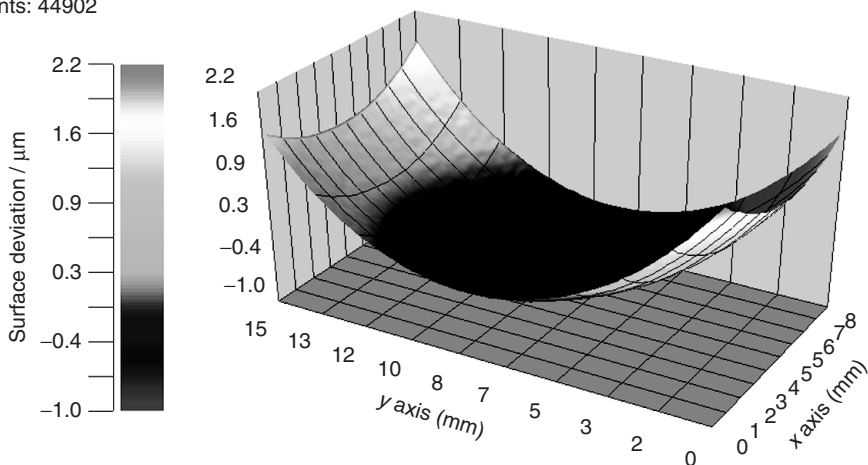
Meas. wavelength = 633 nm

Figure 1.2 Curvature of the microdisplay measured with a Twyman–Green interferometer.

OVT's commercially available 0.7 in. full HD backplane and have been used in numerous adaptive optics applications. HOLOEYE is using nematic LC for their LCOS SLMs with almost analogous phase modulation, because of the higher diffraction efficiency of multilevel hologram structures (256 level, typically 80%). This is one of the main advantages compared with ferroelectric LC (FLC) technology, as FLC can only display binary holograms that always create a symmetrical image leading to a basic 50% loss of light in the system in addition to 50% duty cycle of FLCs. The clear advantage of the FLC is its switching speed, that is, it can be refreshed in the kilohertz range.

1.2.1.2   Signal Flow

In most microdisplay technologies/applications, the signal flow starts with a defined input signal form to be transferred to the microdisplay driver directly in contact with the microdisplay. The schematic representation shown in Figure 1.3 can be used to derive the first batch of parameters leading to an optimized microdisplay drive solution.

Most pixel-based display technologies show a native resolution of a certain display standard (compare, e.g., VESA (Video Electronics Standards Association)), showing optimized performance with input signals representing this native resolution. For higher quality microdisplays, the device can embed the input signal of lower resolution into the physical pixel matrix, filling the whole array of pixels. Pure digital input signals and an EDID (extended display identification data) adapted to the display controllers guarantee the correct choice of timing and addressed display
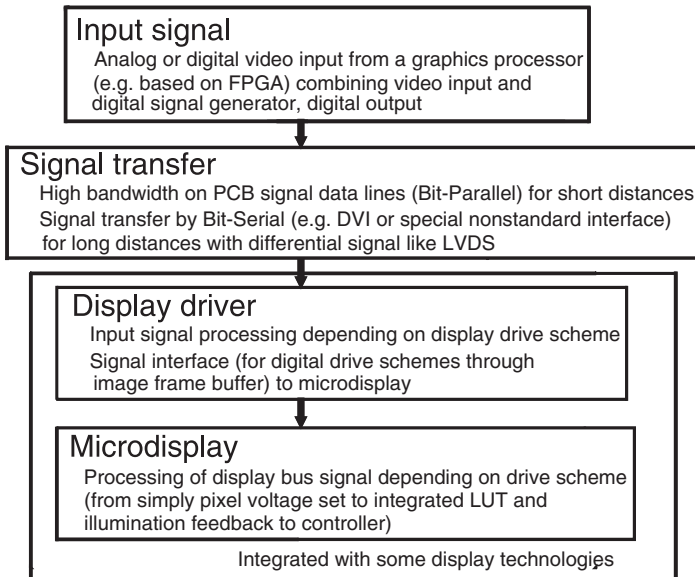
Input signal

Analog or digital video input from a graphics processor
(e.g. based on FPGA) combining video input and
digital signal generator, digital output

Signal transfer

High bandwidth on PCB signal data lines (Bit-Parallel) for short distances
Signal transfer by Bit-Serial (e.g. DVI or special nonstandard interface)
for long distances with differential signal like LVDS

Display driver

Input signal processing depending on display drive scheme
Signal interface (for digital drive schemes through
image frame buffer) to microdisplay

Microdisplay

Processing of display bus signal depending on drive scheme
(from simply pixel voltage set to integrated LUT and
illumination feedback to controller)

Integrated with some display technologies

Figure 1.3 Block diagram of microdisplay driving. LUT, lookup table; PCB, printed circuit board.

resolution. Consumer products are facing the challenge of processing various digital and analog signals, always leading to a compromise in the transferred signal.

Image processors (e.g., based on FPGAs —field-programmable gate array) can combine several input signals and create digital video output according to the capabilities of the display driver technology, leading to a significant design freedom in resolution (aspect ratio), frame rate, and bit depth.

For video-only applications, standard DVI (digital visual interface) and/or HDMI (high-definition multimedia interface) signals provide highest quality, but are rather complex, require a large cable diameter, and cause a relatively high power consumption. Special LVDS (low-voltage differential signal) multiplexer/demultiplexer chipsets are available for custom (frame rate and bit depth) digital signals, such as single pair LVDS transmission solutions, especially for near-to-eye (NTE) applications.

ASIC (application-specific integrated circuit) along with microdisplay combinations (like most HD projection microdisplays) show high flexibility in addressing parameters, but are large and power hungry. Epson and Micron showed more simple approaches, where Epson integrated an LVDS receiver on the microdisplay flex cable (flexible flat cable) and Micron integrated the driver ASIC onto the silicon backplane of the LCOS. The Epson solution can reduce the portion of electronic circuitry right at the microdisplay, so the driver electronics can be separated. The Micron solution (at the moment only up to the resolution of 960×540 pixels) has a fully integrated driver reducing power consumption drastically, but limiting the choice of possible drive schemes.

1.2.1.3 Drive Schemes and Latency

Two major types of drive schemes are used: analog and digital, and this differentiation is based on the actual generated voltage applied to individual pixels.

Analog Drive   In analog drive schemes, the microdisplay utilizes analog voltages directly for the representation of a gray level in an individual LC cell. The scheme is well suited for short illumination pulses because of analog voltages on the pixel (there is no specific digital flicker noise, see further). Analog drive uses typically lower clock frequency and hence has lower power consumption. As a result, longer flex cables between driver and microdisplay are possible.

The analogue scheme also has a number of drawbacks. Drift- and channel-depending variations of drive voltages need to be compensated. The ability for that compensation is evidently limited. The display addressing is progressive, that is, pixels are addressed in a consecutive way and not simultaneously. Effectively, the video signal goes through a low-pass filter. The analog signal path affects the slew rate of the video signal and can superimpose ringing, nonlinear distortion, noise, and echoes. Since the frequency of the video signal is relatively low in the vertical direction and relatively high in the horizontal direction, a significant ''cross talk'' occurs for the latter one, that is, for sequentially written pixels. As a result, a decrease of phase (or amplitude) modulation for high spatial frequencies in the addressed image is observed [17], which corresponds to a decrease in resolution.

The field inversion, which is always required in LCs, in typical analog progressive scan architectures is limited to the single or double frame rate. In the case of the single frame rate field inversion, the DC balancing can fail if the content changes too fast (e.g., due to a specific application). This can cause lifetime issues, that is, destroy the transparent electrode (Indium tin oxide (ITO)). The inversion with the double frame rate requires a frame buffer [18].

Digital Fast Bit-Plane Addressing   In a digital drive scheme a pulse width modulation (PWM) encodes a certain gray level into a series of binary pulses in the kilohertz range, referred to as sequence. In principle, every individual pulse interacts with the LC molecule, causing its rotation, that at the end leads to the desired gray level representation. Owing to limited rotational viscosity of the LC material, LC molecules cannot follow individual pulses of the electrical signal in a discrete way. That is why the base addressing frequency cannot be resolved, so that it is possible to achieve an almost analogous LC molecule position representing/resulting in a certain gray level.

The digital scheme is usually more stable than analog and shows a repeatable performance. Field inversion is possible at the kilohertz range (e.g., for each modulation pulse) without image retention. All pixels are addressed simultaneously. The scheme does not suffer from electrical cross talk (i.e., no low path filtering of the signal). However, an electro-optical cross talk for small pixel sizes may still be observable. The electro-optical cross talk is caused by influence of the electrical field between adjacent pixels and can be further compensated [19].

The control electronics of such microdisplays is compact and has low cost. The device itself is highly programmable. The addressed resolution, amplitude or phase bit depth, and frame rate can be changed *in situ* and if required, adapted to environmental changes (e.g., wavelength, temperature).

The advantages of digital addressing are accompanied by limitations. One observes a kind of flicker noise at high frequencies ("supermodulation"). This means the electro-optical response of the SLM is not constant over the frame. In some scenarios (e.g., projection) time averaging can be used to compensate this effect. In other scenarios, in particular, when using phase modulation or short-pulse light sources, time averaging is not possible. Here, special sequences and higher bandwidth to the LCOS panel help to reduce the flicker noise to acceptable level. Another option is synchronization between the light source and the SLM at the frame rate.

OVT Display Driving   The OVT technology, implemented in HOLOEYE's phase SLMs, uses a digital PWM technique, based on the idea, that a fast sequence of binary modulation can realize an almost analogous response, in particular, for a low bandwidth detector, for example, the human eye. In this way, LC microdisplays with binary modulating FLC material and MEMS technologies, such as digital light processing (DLP), are operated to deliver gray scale modulation. With nematic LC technology, we also have to consider the larger response time of this LC material leading to an almost analogous optical response because of the convolution of the digital pulse code and the LC response time. With OVT's technology [20], it is actually not the "pulse width" that is varied, whereas the gray scale encoding is done by the sequence of bits. The bits of the sequence have individual durations, selected from the set of fixed values. This pulse code modulation (PCM) is advantageous because of the bandwidth limitation and the digital nature of the drive concept. A typical PCM sequence consists of bits with different weights (duration), which are independently programmable, which is repeated every video frame. With this approach, the sequence design offers a lot of flexibility, enabling the microdisplay to be driven with different frame rates, color bit depth, and color frames. Here, a simple 10 bit interface could be used for RGB (sequentially reproduced red, green, and blue) 3 : 4 : 3 bit depth system, which for technical applications shows a quite reasonable performance. For color systems with mainly monochromatic content (e.g., green) a 2 : 6 : 2 bit depth can also be designed and programed.

The effective latency not only depends on the LC response time but also on the drive scheme. The analog drive is typically operated in an "unbuffered" mode, where the pixel data can be directly addressed to the microdisplay. The analog drive uses a progressive scan approach, where there is a continuous serial refresh of the pixel information.

However, the fast bit-plane addressing needs memory for storing the image content. With the incoming video information, the pulse sequence (encoding the gray value) for the individual pixel is written into a frame buffer. With the next frame, binary information for all pixels (the so-called bit planes) is transferred to

all pixels at the same time. The individual gray values are realized with a sufficient number of bit planes.

Most digital drive schemes are designed for video applications, where the human eye is the detector. Any supermodulation (flicker) above 100Hz is almost not noticeable. For applications using a pulsed light source, such as light-emitting diode (LED) or laser, the PWM of the digital display drive could interfere with the light source driving as it was already mentioned above. It is worth mentioning that the electronic addressing bandwidth is the key in defining the right addressing frequency.

1.2.2
Operation Modes

The use of LC materials in SLMs is based on their optical and electrical anisotropy. Typically, a thin layer of LC material can be described as a birefringent material with two refractive indices. The orientation of the index ellipsoid is dependent on the direction of the molecular axis. This orientation is determined by the alignment layers of the LC cell. The most important cases are twisted, parallel aligned (PA), and vertical aligned (VA) cells. In a twisted cell, the orientation of the molecules differs by typically 90° between the top and the bottom of the LC cell and is arranged in a helix-like structure in between. In both PA and VA cells, the alignment layers are parallel to each other, so the LC molecules have the same orientation.

The effect of an LC cell on a monochromatic, polarized light wave can be described by a Jones matrix. Here, ''polarized'' does not necessarily refer to linear polarization, but to a fully polarized state in the sense that the Stokes parameters [21] add up to 1. For PA and VA cells, the Jones matrix [22] is given by

$$W_{\mathrm{PN-LC}} = \exp(-i\phi) \begin{pmatrix} \exp(-i\beta) & 0 \\ 0 & \exp(i\beta) \end{pmatrix} \tag{1.1}$$

where the birefringence β and the phase offset ϕ are given by

$$\beta = (n_{\mathrm{eo}} - n_{\mathrm{o}}) \frac{\pi d}{\lambda} \tag{1.2a}$$

$$\phi = (n_{\mathrm{eo}} + n_{\mathrm{o}}) \frac{\pi d}{\lambda} \tag{1.2b}$$

where n_{o} and n_{e} are the ordinary and extraordinary indices of refraction of the LC material, respectively, d is the thickness of the cell, and λ is the wavelength of the light field. The possibility of changing the birefringence β as a function of the voltage applied to the LC cell makes this component a switchable waveplate.

The Jones matrix of a TN-LC cell is dependent on the physical parameters twist angle, α, front director orientation, ψ, and birefringence, β. It is given by [23]

$$W_{\mathrm{TN-LC}}(f, h, g, j) = \exp -i\phi \begin{pmatrix} f - i \cdot g & h - i \cdot j \\ -h - i \cdot j & f + i \cdot g \end{pmatrix} \tag{1.3}$$

using parameters f, g, h and j which fulfill $f^2 + g^2 + h^2 + j^2 = 1$ and can be calculated from the physical cell parameters as

$$f = \cos \gamma \cos \alpha + \frac{\alpha}{\gamma} \sin \gamma \sin \alpha \tag{1.4a}$$

$$h = \cos \gamma \sin \alpha - \frac{\alpha}{\gamma} \sin \gamma \cos \alpha \tag{1.4b}$$

$$g = \frac{\beta}{\gamma} \sin \gamma \cos(2\psi - \alpha) \tag{1.4c}$$

$$j = \frac{\beta}{\gamma} \sin \gamma \sin(2\psi - \alpha) \tag{1.4d}$$

where the parameter γ is given by

$$\gamma = \sqrt{\alpha^2 + \beta^2} \tag{1.5}$$

The phase factor $\exp(-i\phi)$ can be neglected for most applications. For some commercially available TN-LC-cell-based microdisplays, the parameters α, β, and ψ were not made available by the manufacturers but could be retrieved from optical measurements [24].

It is obvious that the first case of a PA or VA cell is more convenient, at least if we are interested in creating pure phase modulation or polarization modulation.

1.2.2.1 Amplitude Modulation

This modulation type can be achieved with twisted, PA, as well as VA LC cells in a simple optical configuration. The incident light field should be linearly polarized, and after passing through the LC cell, it should be transmitted through a polarizer oriented perpendicular to the incident polarization. For an LCOS-SLM, a polarizing beam-splitter cube is suitable to obtain this. For PA or VA cells, the orientation of the optical axis should be rotated by $45°$ with respect to the incident polarization. For a phase delay of π introduced by the cell, the polarization appears to be rotated by $90°$. The level of attenuation by the second polarizer can be tuned by applying an electric field to the cell, which leads to a change of the birefringence β.

This regime is normally used by projection displays. The three-panel architecture in front projectors can realize very high contrast ratio values above 70 000:1 (JVC DLA-RS series). To get the panels toward fast response time, the VAN mode is used, in which the LC material has a considerable pretilt (also in order to avoid reverse domains), which leads to a residual retardation effect in the dark state, and this needs to be compensated to achieve high contrast ratio. A variety of compensation technologies are available [25, 26], whereas these days, the preferred components are quarter-wave plates (QWPs) and specific retarder plates (see e.g., [22]).

1.2.2.2 Phase Modulation

We have seen that a PA LC cell can be interpreted as a switchable waveplate (Eqs. (1.1) and (1.2a)). It is evident that on transmission through a PA LC cell, light polarized linearly parallel to the extraordinary axis of the LC material is retarded as a function of the voltage-controlled birefringence β (this mode is also known

as *ECB*). Therefore, such cell is a convenient phase-only modulator for linearly polarized light.

Obtaining phase-only modulation using twisted cells is significantly more complicated. It has been shown that there are elliptic polarization states that are only subject to phase modulation, with tolerable amplitude modulation introduced by a polarizer behind the SLM [27, 28]. This mode of operation is often referred to as phase-mostly operation. Creating the appropriate elliptic polarization requires a QWP, as well as the conversion to a linearly polarized state behind the SLM.

This regime has many applications ranging from wavefront control (with typically slowly varying phase functions) to dynamic computer-generated holography (with typically fast spatial variation of the phase function). In the latter case, a suitable algorithm for the creation of the phase-only hologram is required. Such computational algorithms have been adapted to match the particular needs of SLM applications in order to deal with fringe field effects, [29], optimize the speed of holographic computations [30], obtain a free choice of diffraction angles [31], and reduce the intensity fluctuations during frame-to-frame SLM update [32].

1.2.2.3 Polarization Modulation

When placing a waveplate of variable retardance ("WP1") between two QWPs, with the optical axes of these QWPs rotated by $+45°$ and $-45°$ with respect to the optical axis of WP1, the Jones matrix of the three waveplates together is a rotation matrix in which the rotation angle is given by the phase shift of WP1. Therefore it is possible to convert a phase modulating SLM into a 2D matrix of phase-rotating pixels by sandwiching it between two such QWPs. Interestingly, the polarization rotating feature is not dependent on the polarization of the incident light wave, only on the degree of polarization, which should be 1, and its wavelength. To give an example, this means that by addressing a vortex phase function to the SLM, a linearly polarized beam can be converted into a beam with radial or azimuthal polarization.

1.2.2.4 Complex-Valued Modulation

A desired mode of operation would be the ability to change both amplitude and phase of an incoming wavefront simultaneously, thereby creating a complex-valued transmittance of the SLM. From the discussion above it is evident that while of course phase and amplitude can be modulated by a single cell, the amplitude and phase values cannot be chosen independently, which makes complex-valued operation using a single cell almost unusable. Following are the options to represent a complex-valued transmittance by using special configurations.

• Stacking two LC cells: This involves sandwiching two LC layers and operating one in phase-only and the the other in amplitude-only mode. A transmissive SLM with a 1D array of pixels is manufactured by Cambridge Research and Instrumentation, but for 2D arrays of pixels the control of the two independent voltages required for each pixel has prevented the realization of such device.
• 4f imaging: In this option two SLM devices, including polarizer(s), with two lenses in 4f configuration are used and one device is operated in phase-only

and the other in amplitude-only mode (or vice versa),. Apart from the spatial frequency bandwidth limitation and inevitable optical aberrations, this would be the straightforward equivalent to physically stacking two LC cells.

- Macro pixel technique: In this, two adjacent pixels can be used to represent the real and imaginary parts of the desired complex transmittance [33] or can be combined together with help of additional thin components, which provides better quality of reconstruction in digital holography [34]; three amplitude pixels can very well represent a complex value [35], and using four pixels, it is possible even to use TN cells with mixed polarization and phase modulation [36].
- Spatial multiplexing: In the special case that the desired complex distribution is the sum of two phase functions it is an option to use a single phase-only SLM and to display each phase function in only every second of the available pixels. The pixel locations used for each phase function can simply be a random pattern [37].

1.2.3
Performance Evaluation

The evaluation of the SLM performance for digital holography applications typically comprises evaluation of phase response versus addressed value (linearity and maximal achievable phase delay) as well as phase response versus time, crosstalk versus spatial frequencies, flatness of the display, response times, and cross modulation.

Phase response can be measured using a Michelson interferometer or also with a common path interferometer [38]. Alternatively, it is possible to get a good estimation indirectly, using amplitude modulation mode. In this case, the incident polarization is oriented at 45° to the slow axis (in phase mode, it is parallel) and the analyzer is set perpendicular to the incident polarization. However, the advantage of a Michelson interferometer is that it is well suited for determining the flatness of the SLM at the same time (Figure 1.2).

Measurement of the phase response requires a high-speed detector, because the specific digital noise has relatively high frequency. One indirect method is to address diffraction gratings to the SLM and to observe intensity of the diffraction orders with a single detector (photodiode), attached to an oscilloscope. This method actually measures the diffraction efficiency over time. Another indirect method is to use an amplitude modulation mode, that is, to measure intensity noise over time. A more direct measurement can be performed using an interferometer with fast acquisition or with a stroboscopic technique [39].

Cross talk can be well evaluated with a simple approach, in which diffraction efficiency is measured versus addressed phase value for different spatial frequencies. The resulting curves can be used to derive actual phase modulation of the addressed grating versus addressed values [38].

Cross modulation is a residual amplitude modulation, which accompanies phase modulation. Residual amplitude modulation means that light coming from the SLM has a certain ellipticity in polarization state. This is simple to measure using

an analyzer, which is oriented parallel to the incident polarization, and a power meter. More generally, as mentioned above, a full Jones matrix can be determined and taken into account later in the calculation of holograms [40, 41]. Response times can be basically evaluated with an oscilloscope and photodiode, observing diffraction order intensity of an addressed grating (the grating is then switched on and off). Alternatively, measurements in amplitude modulation mode as well as time-resolved phase measurements can be considered (as already mentioned).

Also of importance is the quality of anti-reflection (AR) coating of the front and back surfaces of the cover glass. Parasite reflections created by one of this surfaces can cause Fabry-Pérot-type interferences in the microdisplay.

For industrial and high-power applications, the behavior of SLM in response to temperature can be important. It is defined mainly by the dependence of the viscosity of the LC material on temperature. Higher temperatures usually decrease response times and increase phase modulation values at the cost of increasing temporal noise.

1.3
Some Applications of Spatial Light Modulators in Optical Imaging and Metrology

SLMs are used in a wide variety of applications mostly as a phase modulator, among which are measurement systems, microscopy, telecommunications, and digital holography. Meeser *et al.* [42] developed a holographic sensor, using an SLM to adapt the reference wave for different object positions as well as a flexible phase shifter. The SLM allows to switch between Fresnel and Fourier holograms and to determine accurately the phase distribution in the CCD plane using phase shifting algorithms (Figures 1.4 and 1.5). Another system from the same group works using
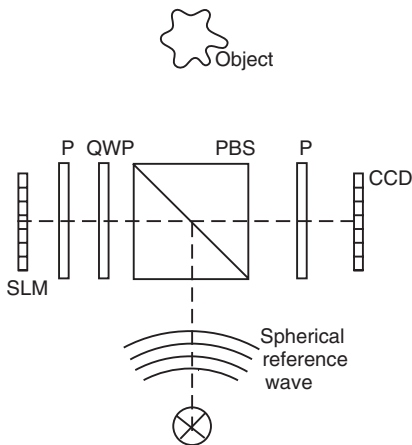
Figure 1.4 Schematic layout of the holographic sensor. P, polarizer; QWP, quarter-wave plate; PBS, polarizing beam splitter; CCD, detector. (Source: Adapted with permission from [42].)
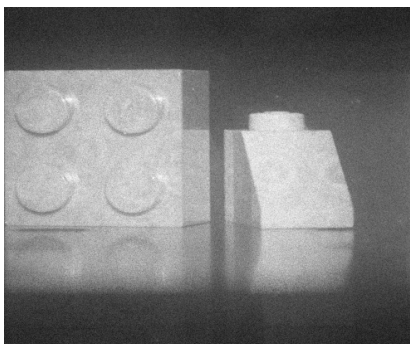
Figure 1.5 Numerical reconstruction of the hologram, captured with the holographic sensor. Source: With permission from [42].

the shearography principle, where the SLM performs the function of a shear [43], see also Chapter 17. Schaal *et al*. [44] proposed to use a phase SLM in a multipoint dynamic vibrometer, where the vibration is simultaneously measured in a freely selectable set of points. Baumbach *et al*. [45] demonstrated a digital holography technique, which replaces the holographic interferometry and implements SLM for achieving ''analog'' optical reconstruction of the master object.

Jenness [46] demonstrated the use of a phase SLM in a holographic lithography system (Figure 1.6), in which he successfully processed micropyramid structures (Figure 1.7) in photoresist [47, 48]. The main limitation of lithography applications with LCOS is the UV absorption of the LC cell, which does not allow the use of short wavelengths and hence affects the increase of the resolution of the lithography. Even though there exist transmission windows in the absorption spectrum [49, 50], the use of these windows does not look feasible. More flexible might be a combination of holographic lithography with two-photon lithography [51], which gives the possibility of working in the visible spectrum and then halving the wavelength due to the two-photon effect in the object plane. A similar principle was used in the realization of scanless two-photon microscopy by Nikolenko *et al*. [52]. Another maskless lithography application that utilizes polarization modulation in the SLM plane, which is imaged onto the object plane (a photoactive polymer film), is the fabrication of polarization computer-generated holograms (CGHs) [53].

The capability of LCOS to withstand high light intensities (that is actually inherited from its ''front projection'' origin), permits unusual LC applications. Kuang *et al*. [54] directly used a high-power laser to make microstructuring with laser ablation parallel at many points of an array. Nevertheless, the SLM function in this case is similar to holographic lithography described before.

Microscopic applications of SLMs have been found in the illumination or in the imaging light path. Examples for SLM usage in the illumination path are structured illumination microscopy [56–58], optical tweezing, and point spread function (PSF)-engineering (discussed below). Use of LC SLMs for optical tweezing was first proposed by Hayasaki *et al*. [59], followed by a number of publications of Dufresne and Grier [60], Reicherter *et al*. [61]. Figure 1.8a shows optical tweezer

Microscope

Condenser

1.4 NA, 100×
objective, f_{obj}

L_6

L_5

M_4

DBS

Filter

TL

CCD camera

M_2

L_4

M_3

M_1

L_3

SLM

Half waveplate
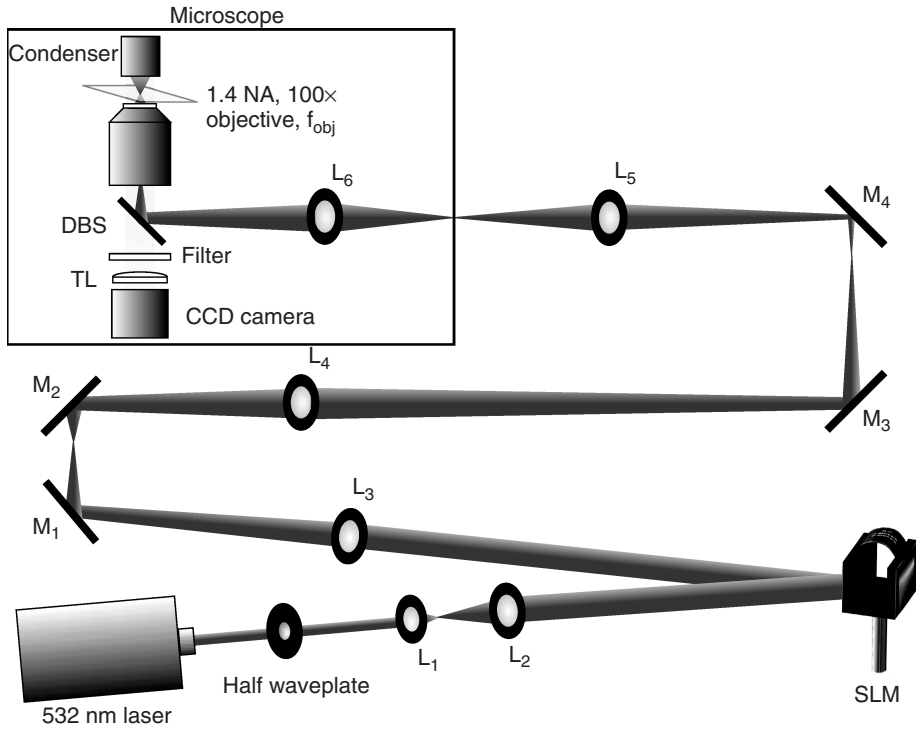
L_1

L_2

532 nm laser

Figure 1.6 Schematic layout of the holographic lithography system. M1–M4, fold mirrors; L1 and L2, beam expander; L3–L6, relay lenses. DBS, dichroic beam splitter; TL, tube lens. Source: With permission from [46].
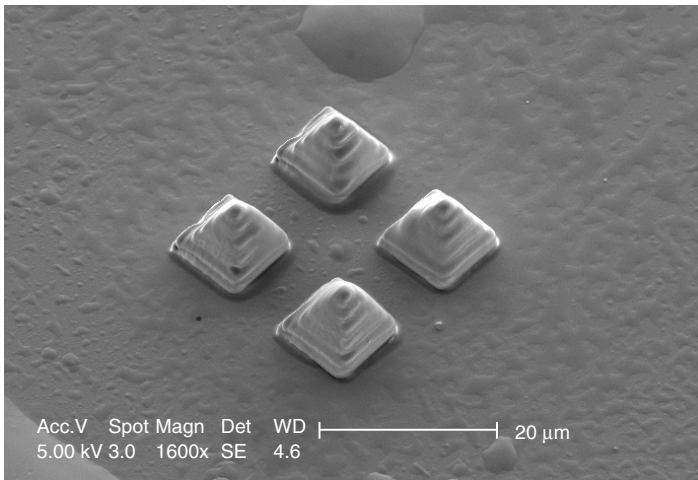
| Acc.V | Spot | Magn | Det | WD | | 20 μm |
| 5.00 kV | 3.0 | 1600x | SE | 4.6 | | |

Figure 1.7 Processed structure. Source: With permission from Ref. [46].

(a)

(b)
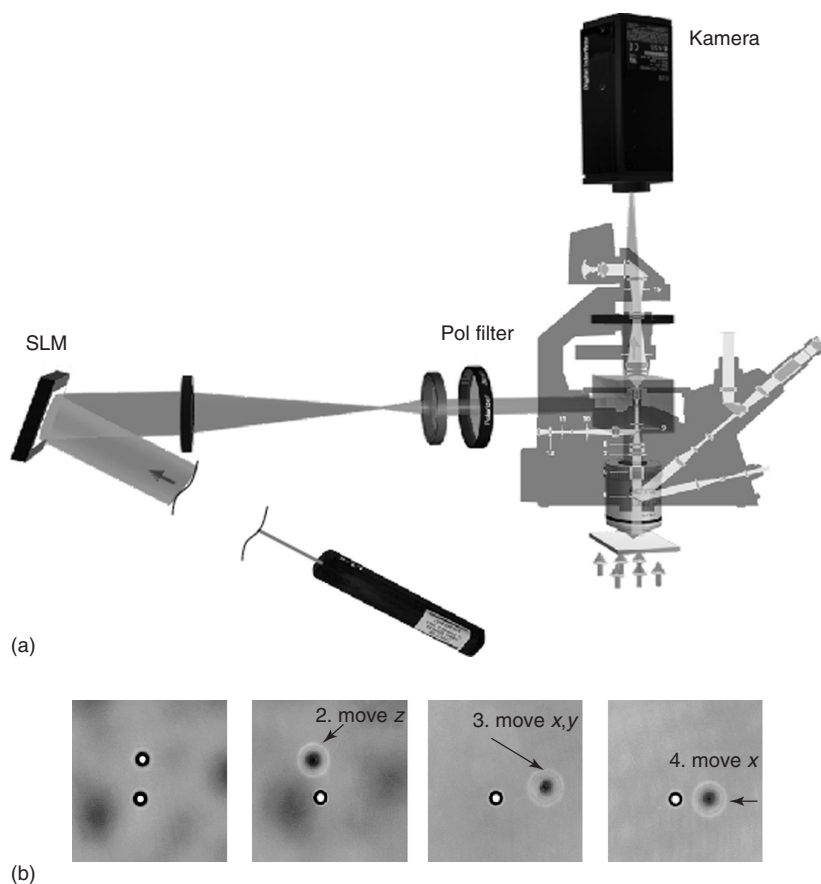
Figure 1.8 Optical tweezing system. (a) Schematic layout. (b) One particle is trapped in *x-y-z* relative to another particle. Source: With permission from Institut für Technische Optik, Stuttgart. (a) Taken from [55].

setup integrated in a Zeiss Axiovert 200. The SLM is telecentrically imaged into the pupil of the microobjective lens. The object is then illuminated with a pattern, which reconstructs a hologram addressed to the SLM. Moving of optical traps (i.e., addressing holograms to SLM) allows to move one or multiple objects in three dimensions (Figure 1.8b), see [62]. The state of the art in holographic optical tweezing is reviewed in Chapter 8.

For application in the imaging light path, LCOS SLMs were used in implementations of a phase contrast microscope [63–65], where addressing of different phase patterns to the SLM located in the Fourier plane allowed to get phase contrast, DIC (differential interference contrast), and dark field images in the same microscope (Figure 1.9). Figure 1.10 shows a phase bar structure imaged in bright field in panel (a) and SLM-based DIC in panels (b and c). The difference between two DIC images in Figure 1.10 represents two different periods of the gratings used for DIC.
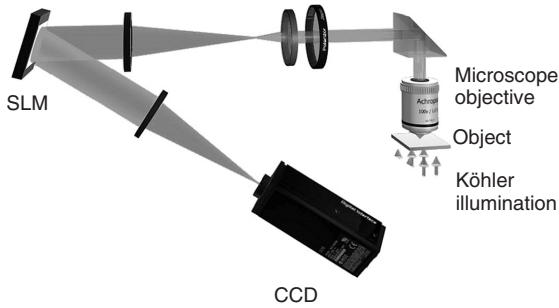
Figure 1.9 Schematic layout of the implementation of phase contrast. Source: With permission from [63].
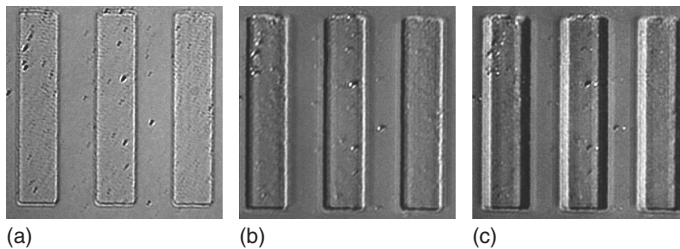

Figure 1.10 Phase object imaged with bright field (a) and DIC (b,c). Source: With permission from [63].

Another attractive application is coherence holography proposed by Takeda *et al.* [66], also see Chapter 11. This principle was originally proposed for microscopy [67], which allows to eliminate dispersion problems [68], see also Chapter 6. The same idea was recently applied for a synthetic aperture telescope [69].

One can find an excellent review of the SLM applications in microscopy in a recent paper by Maurer *et al.* [70].

Very promising are advances in application of phase SLMs in superresolution microscopy. Auksorius *et al.* [72] generated and controlled a doughnut-shaped PSF of a stimulated emission depletion (STED) beam with a phase SLM. They showed rapid switching between different STED imaging modes as well as correction of aberrations in the depletion path of the microscope and achieved significant resolution improvement compared with the standard confocal technique (Figure 1.11). The compensation of aberrations is especially important because of high sensitivity of the STED beam [71]. The standard confocal method can be also improved – as it was proposed recently by Mudry *et al.* [73], confocal microscopes could significantly increase resolution in z-axis, using an SLM for generation of two superimposed spots, which results in an isotropic diffraction-limited spot. These applications are very close to the more general method, called *SLM-based PSF engineering* [74].

PSF engineering is the most common use of LCOS SLMs operated in a mode to provide polarization modulation. Generation of polarization patterns [75–77] already found plenty of applications in microscopy, giving the possibility to reduce
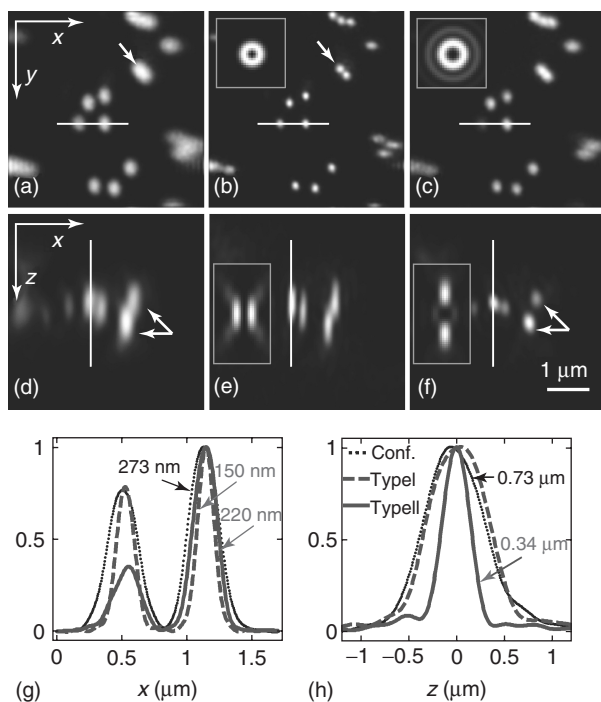
Figure 1.11 (a,b,c) Lateral and (d,e,f) axial fluorescence images of 200 nm beads with (a,d) confocal acquisition, (b,e) acquisition with a doughnut STED beam (type I), and (c,f) acquisition with a "bottle" STED beam (type II). (g,h) Normalized intensity line profiles of lateral and axial images, respectively, with specified FWHM. Insets show the corresponding PSFs. Note the differences in lateral and axial resolution between two STED imaging modes. (Source: With permission from [71]). (Please find a color version of this figure on the color plates.)

a spot size [78], to generate a doughnut, an optical bubble [79], or needle [80]. Generation of the doughnut could also be achieved with spiral phase pattern without additional polarization components (e.g., QWPs) as it was discussed earlier [72, 81]. Beversluis and Stranick [82] showed independent polarization and phase modulation with two SLMs, which succeeded in increasing the contrast of 300 nm polystyrene beads in coherent anti-Stokes Raman spectroscopy (CARS) images. They used independent phase and polarization modulation (Figure 1.12) for PSF engineering (Figure 1.13, see also [74]). SLM 1 in Figure 1.12 performs phase-only modulation of the light wave. SLM 2 with attached QWP is dedicated to polarization-only modulation. These two SLMs with optics form a "mode converter," so that finally phase- and polarization-modulated wavefronts are telecentrically imaged in the pupil plane of the microobjective lenses. The differences between linear, azimuthal, and radial polarizations showed in Figure 1.13 are obvious. Note also the changes in the Z-component of the field.

The methods and applications of PSF engineering were recently reviewed by Zhan [83].
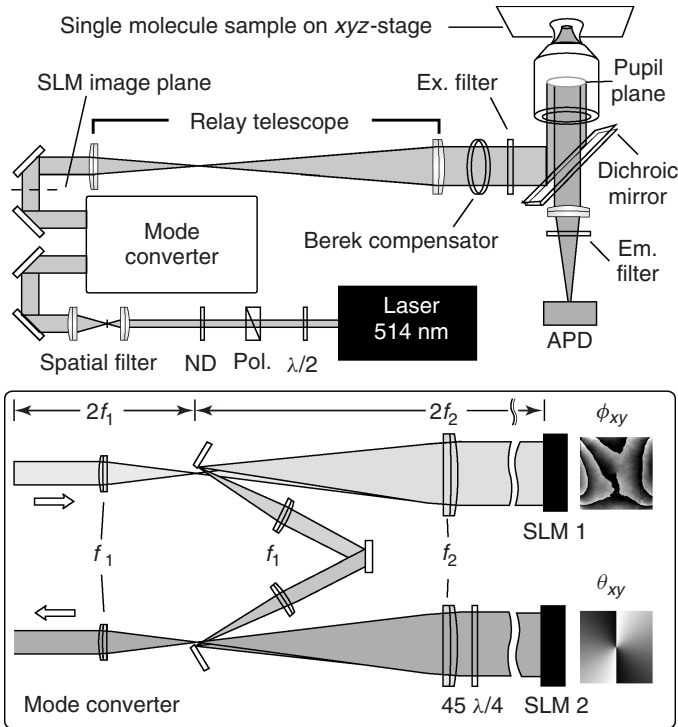
Figure 1.12 Schematic layout of the phase and polarization modulation in a PSF-engineered microscope. Source: With permission from [74].
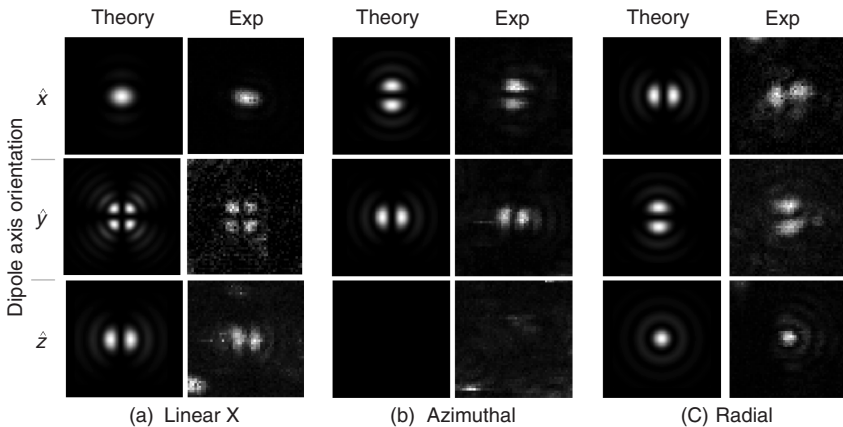

Figure 1.13 Theoretical and experimental images for (a) linear, (b) azimuthal, and (c) radial pupil polarizations (each image has 2 μm side). Source: With permission from [74].
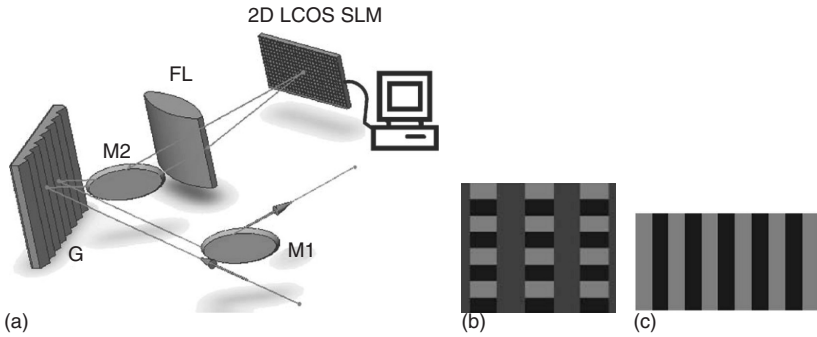
Figure 1.14 Femtosecond pulse shaper. (a) Schematic layout. G, diffraction grating; M1 and M2, mirrors; FL, Fourier lens. (b) Amplitude modulation with SLM. (c) Phase modulation with SLM. Source: With permission from [84].
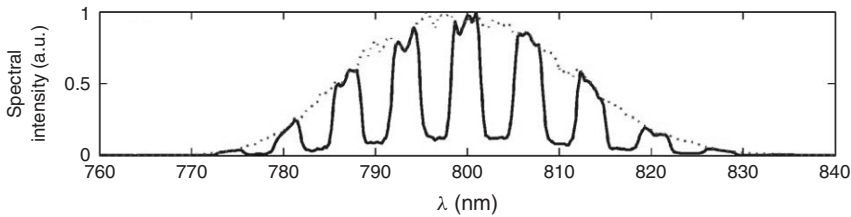

Figure 1.15 Amplitude-only modulation of the spectrum. Source: With permission from [84].

Frumker and Silberberg [84] demonstrated amplitude and phase shaping of femtosecond laser pulse using an LCOS phase modulator (Figure 1.14a). Here illumination femtosecond pulses are split into a spectrum with help of a grating G so that a cylindrical Fourier lens FL focuses each wavelength component onto the SLM in only one direction. The components stay in the same time spread in vertical direction. Then, writing a phase grating in vertical direction (Figure 1.14b) allows to modulate amplitude of the spectral components (Figure 1.15) independent of the phase modulation (the last one uses SLM in horizontal direction – Figure 1.14c). The phase modulation is observed as a correlation function showed at Figure 1.16. A principle capability of LCOS to work in the near-infrared range allowed to develop a telecommunication device based on a similar principle, combining optical switching [85] and pulse shaping capabilities of SLMs [86]. A similar approach was recently patented and commercialized by Finisar [87].

There are several attempts to use SLM for holographic reconstruction in visual systems. A comprehensive review of SLM-based holographic 3D displays is given by Onural *et al.* [89]. SeeReal Technologies demonstrated an 8 in. full color holographic projection 3D display (Figures 1.17 and 1.18) using an amplitude SLM and observation through a concave mirror – ''display'' [88]. The color was achieved using color field sequential technology. The holograms were a kind of Fresnel hologram, where complex values were converted to amplitude values using well-known
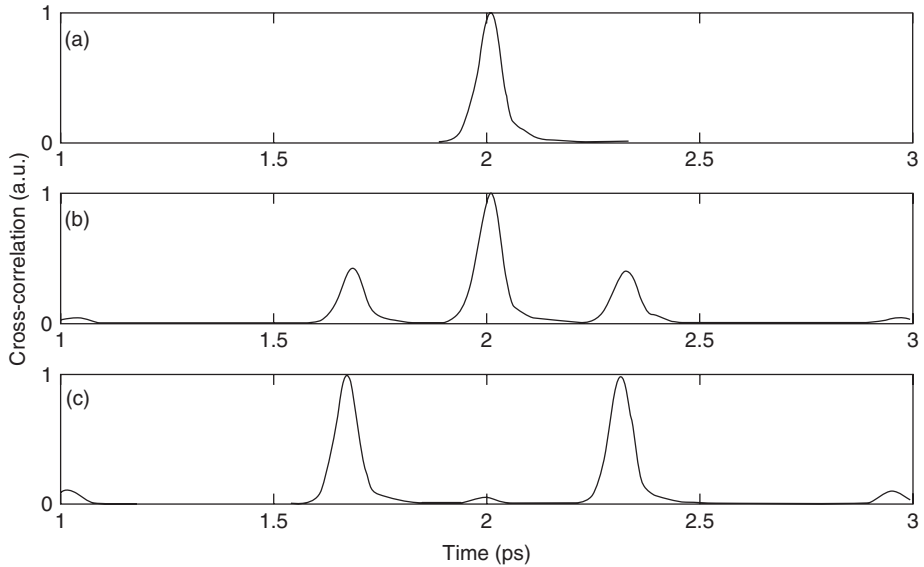
Figure 1.16 Cross-correlation. (a) No phase is applied. (b) Periodic phase-only modulation with binary modulation depth of $\pi/2$ and period 3.1 THz. (c) Periodic phase-only modulation with modulation depth of π. Source: With permission from [84].
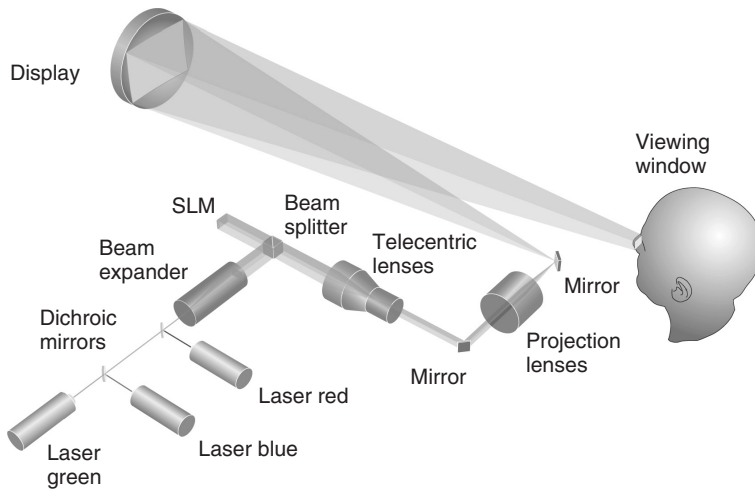

Figure 1.17 Schematic layout of 3D projection display. Source: With permission from [88].

Burckhardt or detour phase encoding [35]. A significant drawback of the system is its relatively low light efficiency, caused by the usage of an amplitude SLM. This is an unusual example of using amplitude modulation in digital holography, as 3D displays of this kind are thought to be realized with a phase modulator. However,

Figure 1.18 Photo of the display. (Source: With permission from [88]). (Please find a color version of this figure on the color plates.)

here the amplitude modulation provided good-quality reconstructions and helped to omit iterative calculations at the same time.

Light Blue Optics introduced full color 2D holographic projection unit with ferroelectric SLMs [90]. They demonstrated good quality of reconstructions, using high frame rate of ferroelectric SLMs to suppress perceivable speckle noise. Unfortunately, due to the nature of ferroelectric LCs, as it was already mentioned above, this approach shows relatively low light efficiency.

An implementation of the holographic visualization in the head mounted display (HMD) looks quite attractive as well. The features would be high brightness and capability of 3D representing information or objects overlapped with real objects (see-through). The reconstructed information can be adapted to the individual observer using the wavefront correction properties and thus will allow to compensate myopia or hyperopia, astigmatic errors of the eye, as well as other aberrations up to ''supernormal vision'' level as it was demonstrated by Liang *et al.* [91].

The basic layouts for the HMD can be different, e.g., projection of the SLM into the eye pupil, as it was already demonstrated for head-up display [92] or the projection of the Fourier transform of the SLM, as it was made in the projection holographic display of SeeReal Technologies (see earlier discussion). Main parameters of the HMD are the exit pupil and the FOV. Simple analysis shows that the product of the FOV and exit pupil in a digital holographic HMD is an invariant quantity that is proportional to the number of pixels at the SLM, regardless of the scheme used (as long as no pupil expander is used). This means that visual holographic systems are very critical to pixel count so that system becomes feasible only if the pixel amount exceeds 2–4 megapixels. Figures 1.19 and 1.20 show reconstructions from a prototype of a digital holographic see-through HMD, based on phase-only HOLOEYE SLM of the high-definition television (HDTV) resolution and a fiber-coupled red superluminescent diode. The numerical aperture of the camera was matched to that of the human eye. This ensures similarity of speckle characteristics between the captured pattern and the pattern perceived by the
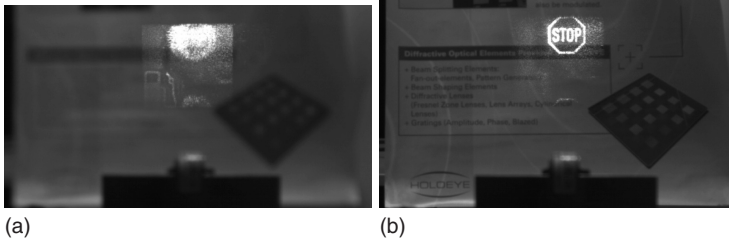
(a)   (b)

Figure 1.19 Reconstruction of a hologram, captured at two reconstruction distances. The FOV is ≈6° in horizontal and 3.4° in vertical direction. The exit pupil is 12 mm. Note the difference in acuity of the background. (a) Fuel sign. (b) Stop sign.
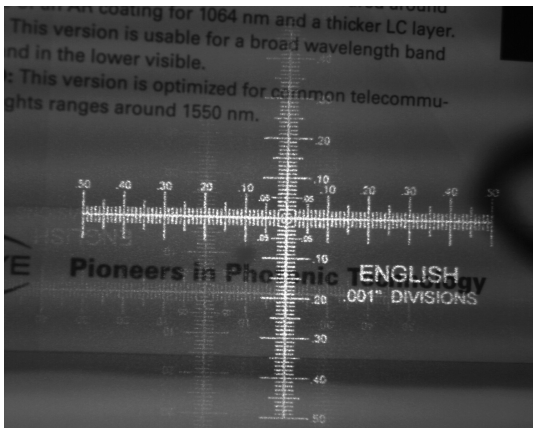

Figure 1.20 Reconstruction of a resolution test target. Field of view is ≈14°.

human eye [93]. The SLM is projected in the exit pupil plane with help of a telecentric system. The observer's eye makes a Fourier transform and gets an image at the retina. Figure 1.19a,b is the reconstruction from the same hologram. The hologram contains 3D information, which is reconstructed in two different planes. Another example shows approximately 14° field of view (Figure 1.20), where the eye can resolve a finer pattern.

The 3D display application, realized as an array of phase SLMs with Fresnel holograms, is given in Chapter 3. The readers are also referred to Chapter 2 for a general overview of the 3D display technologies.

In addition to the more established fields of applications such as microscopy, metrology, and holographic visualization, there is an apparently ever-growing number of other fields in which the potential benefits of using SLMs are expected. It can relate to optical processing of the information; for example, Marchese *et al.* [94] designed an SLM-based optronic processor for rapid processing of the synthetic-aperture radar (SAR) multilook images. As an adaptive optics example, Vellekoop and Mosk [95] focused light through a highly scattering medium. There are a number of scientific works, related to quantum optics. Becker *et al.* [96]

applied amplitude SLM to generate dark solitons in Bose−Einstein Condensate (BEC), whereas another group manipulated BEC with a ferroelectric phase SLM [97]. Bromberg *et al.* [98] implemented computational ghost imaging with only a single bucket detector, where the rotating diffuser was replaced with a phase SLM, thus allowing the computation of the propagating field and omitting the usage of the second high-resolution detector. Stütz *et al.* [99] generated, manipulated, and detected multidimensional entangled photons with a phase SLM. Following him Lima *et al.* [100] demonstrated manipulation with spatial qudit (''multilevel qubit'') states.

1.4
Conclusion

LC-based SLMs have existed for the past 40 years and have been a basis for many studies in electro-optical effects. With the reflective LCOS microdisplay technology, one could realize components with parameters, unthought before (e.g., resolution, pixel size, fill factor, overall light efficiency, and driving electronics solutions).

Even though projection display and SLM target markets are quite different, trends in the LCOS microdisplay technology fit to some extent the requirements of SLM development. This fact, the accessibility of the technology, and the possibility of customization of the parameters also lead to considerably smaller investments. The background in consumer products also ensures achievement of stable, predictable, and high-performance commercial products with competitive pricing.

The availability of such SLMs has helped the scientific community to explore a wide range of potential applications. High-resolution devices were made possible, but for phase modulators, high diffraction efficiency along with high frame rate is still a challenge. Customization including SLM-specific backplane design together with mass-production-suitable production facilities opens the way for implementation in various commercial applications.

Current developments will bring 10 megapixel phase-only panels (e.g., 4160 × 2464 pixels) to the market. Pixel size will drop down further below 4 μm. The continuous progress in the development of driving electronics makes higher refresh rates available, together with a reduction of digital-specific noise. This will positively influence feasibility of SLMs for industrial applications.

Although LCOS SLMs have originally found their applications in scientific research, there is an increased interest in the commercial field and a transition from science to industry is expected in the near future.

References

1. Solgaard, O. (2009) *Photonic microsystems: micro and nanotechnology applied to optical devices and systems,* Springer.
2. Armitage, D., Underwood, I., and Wu, S.-T. (2006) *Introduction to Microdisplays,* John Wiley & Sons, Ltd, Chichester.
3. Knipe, R.L. (1996) Challenges of a digital micromirror device: modeling and design. SPIE Proceedings Micro-Optical

Technologies for Measurement, Sensors, and Microsystems, vol. 2783, pp. 135–145. doi: 10.1117/12.248483.

4. Amm, D.T. and Corrigan, R.W. (1998) Grating light valve technology: Update and novel applications. *SID Symp. Dig. Tech. Pap.*, **29** (1), 29–32. doi: 10.1889/1.1833752.

5. Schenk, H., Wolter, A., Dauderstaedt, U., Gehner, A., and Lakner, H. (2005) Micro-opto-electro-mechanical systems technology and its impact on photonic applications. *J. Microlith. Microfab. Microsyst.*, **4** (4), 041501. doi: 10.1117/1.2131824.

6. López, D., Aksyuk, V.A., Watson, G.P., Mansfield, W.M., Cirelli, R., Klemens, F., Pardo, F., Ferry, E., Miner, J., Sorsch, T.W., Peabody, M., Bower, J., Peabody, M., Pai, C.S., and Gates, J. (2007) Two-dimensional MEMS array for maskless lithography and wavefront modulation. *SPIE Proc.*, **6589**,. doi: 10.1117/12.724467.

7. Lapisa, M., Zimmer, F., Niklaus, F., Gehner, A., and Stemme, G. (2009) Cmos-integrable piston-type micro-mirror array for adaptive optics made of mono-crystalline silicon using 3-d integration. Proceedings of the IEEE International Conference on Micro Electro Mechanical Systems, pp. 1007–1010.

8. Doucet, M., Picard, F., Niall, K.K., and Jerominek, H. (2005) Operation modes for a linear array of optical flexible reflective analog modulators. SPIE Proceedings Cockpit and Future Displays for Defense and Security, vol. 5801, pp. 219–233. doi: 10.1117/12.604059.

9. Melcher, R.L. (2000) LCoS microdisplay technology and applications. *Inform. Display*, **16** (7), 20–23.

10. Fournier, F.R. and Rolland, J.P. (2008) Design methodology for high brightness projectors. *J. Display Technol.*, **4** (1), 86–91.

11. Sterling, R. (2008) JVC D-ILA high resolution, high contrast projectors and applications. *Proceedings of the 2008 Workshop on Immersive Projection Technologies/Emerging Display Technologies*, ACM, New York USA, pp. 10: 1–10:6.

IPT/EDT '08, ISBN 978-1-60558-212-2. doi: 10.1145/1394669.1394684.

12. Fujitsu Semiconductor Ltd (2007) Wafer foundry service. FIND Vol.25 No.1.

13. Neil Savage (2009) Digital spatial light modulators. *Nat. Photon.*, **3** (3), 170–172.

14. Cuypers, D., Van Doorselaer, G., Van Den Steen, J., De Smet, H., and Van Calster, A. (2002) Assembly of an XGA 0.9 LCOS display using inorganic alignment layers for VAN LC. Conf. Rec. Int. Disp. Res. Conf., Society for Information Display (SID), pp. 551–554.

15. Gandhi, J., Anderson, J.E., and Stefanov, M.E. (2001) Experimental comparison of contrast ratio vs. f/# for various reflective LCoS modes. *SID Symp. Dig. Tech. Pap.*, **32** (1), 326–329. doi: 10.1889/1.1831862.

16. Osten, S., Krüger, S., and Hermerschmidt, A. (2008) New HDTV (1920 × 1080) phase-only SLM, in *Adaptive Optics for Industry and Medicine* (ed. C. Dainty), SPIE, pp. 124–129.

17. Márquez, A., Iemmi, C., Moreno, I., Campos, J., and Yzuel, M. (2005) Anamorphic and spatial frequency dependent phase modulation on liquid crystal displays. optimization of the modulation diffraction efficiency. *Opt. Express*, **13** (6), 2111–2119. doi: 10.1364/OPEX.13.002111.

18. Karl Waterman, J. (2007) Display driver architecture for a liquid crystal display and method therefore. US Patent 7161570.

19. Worley, S.W. and Hong Chow, W. (2010) System and method for reducing inter-pixel distortion by dynamic redefinition of display segment boundaries. EP Patent 1093653 B1.

20. Spencer Worley, W., Lyle Hudson, E., and Hong Chow, W. (2008) Display with multiplexed pixels and driving methods. US Patent Application 2008/0225030.

21. Shurcliff, W.A. (1962) *Polarized Light, Production and Use*, Harvard University Press.

22. Robinson, M., Sharp, G., and Chen, J. (2005) *Polarization Engineering for LCD Projection*, John Wiley & Sons, Ltd, Chichester.

23. Yariv, A. and Yeh, P. (1984) *Optical Waves in Crystals*, John Wiley & Sons, Inc., New York.

24. Hermerschmidt, A., Quiram, S., Kallmeyer, F., and Eichler, H.J. (2007) Determination of the Jones matrix of an LC cell and derivation of the physical parameters of the LC molecules. *SPIE Proc*, **6587**,. doi: 10.1117/12.722895.

25. Duelli, M., Shemo, D.M., Hendrix, K.D., Ledeur, A., and Tan, K.L. (2005) High performance contrast enhancing films for VAN-mode LCOS panels. *SID Sympo. Dig. Tech. Pap.*, **36** (1), 892–895. doi: 10.1889/1.2036592.

26. Tan, K.L., Hendrix, K.D., Duelli, M., Shemo, D.M., Ledeur, A., Zieba, J., and Greenberg, M. (2005) Design and characterization of a compensator for high contrast LCoS projection systems. *SID Symp. Dig. Tech. Pap.*, **36** (1), 1810–1813. doi: 10.1889/1.2036370.

27. Davis, J.A., Moreno, I., and Tsai, P. (1998) Polarization eigenstates for twisted-nematic liquid-crystal displays. *Appl. Opt.*, **37** (5), 937–945.

28. Clemente, P., Durán, V., Martínez-León, Ll., Climent, V., Tajahuerce, E., and Lancis, J. (2008) Use of polar decomposition of Mueller matrices for optimizing the phase response of a liquid-crystal-on-silicon display. *Opt. Express*, **16** (3), 1965–1974.

29. Milewski, G., Engström, D., and Bengtsson, J. (2007) Diffractive optical elements designed for highly precise far-field generation in the presence of artifacts typical for pixelated spatial light modulators. *Appl. Opt.*, **46** (1), 95–105. doi: 10.1364/AO.46.000095.

30. Georgiou, A., Christmas, J., Collings, N., Moore, J., and Crossland, W.A. (2008) Aspects of hologram calculation for video frames. *J. Opt. A: Pure Appl. Op.*, **10**, 035302. doi: 10.1088/1464-4258/10/3/035302.

31. Hermerschmidt, A., Krüger, S., and Wernicke, G. (2007a) Binary diffractive beam splitters with arbitrary diffraction angles. *Opt. Lett.*, **32** (5), 448–450. doi: 10.1364/OL.32.000448.

32. Persson, M., Engström, D., Frank, A., Backsten, J., Bengtsson, J., and Goksör, M. (2010) Minimizing intensity fluctuations in dynamic holographic optical tweezers by restricted phase change. *Opt. Express*, **18** (11), 11250–11263. doi: 10.1364/OE.18.011250.

33. Birch, P.M., Young, R., Budgett, D., and Chatwin, C. (2000) Two-pixel computer-generated hologram with a zero-twist nematic liquid-crystal spatial light modulator. *Opt. Lett.*, **25** (14), 1013–1015. doi: 10.1364/OL.25.001013.

34. Fütterer, G., Leister, N., Häussler, R., and Lazarev, G. (2010) Three-dimensional light modulation arrangement for modulating a wave field having complex information. Patent Application WO 2010/149588 A1.

35. Burckhardt, C.B. (1970) A simplification of Lee's method of generating holograms by computer. *Appl. Opt.*, **9** (8), 1949–1949. doi: 10.1364/AO.9.001949.

36. van Putten, E.G., Vellekoop, I.M., and Mosk, A.P. (2008) Spatial amplitude and phase modulation using commercial twisted nematic LCDs. *Appl. Opt.*, **47** (12), 2076–2081. doi: 10.1364/AO.47.002076.

37. Rosen, J. and Brooker, G. (2007) Digital spatially incoherent Fresnel holography. *Opt. Lett.*, **32** (8), 912–914. doi: 10.1364/OL.32.000912.

38. Hermerschmidt, A., Osten, S., Krüger, S., and Blümel, T. (2007) Wave front generation using a phase-only modulating liquid-crystal-based micro-display with hdtv resolution. SPIE Proceedings, Adaptive Optics for Laser Systems and Other Applications, vol. 6584, p. 65840E. doi: 10.1117/12.722891.

39. Emery, Y., Cuche, E., Marquet, F., Aspert, N., Marquet, P., Kuhn, J., Colomb, T., Montfort, F., Charriere, F., Depeursinge, C., Debergh, P., and Conde, R. (2006) Digital holographic microscopy (dhm) for metrology and dynamic characterization of mems and

moems. *SPIE Proc.*, **6186**, 61860 N. doi: 10.1117/12.660029.

40. Kohler, C., Haist, T., Schwab, X., and Osten, W. (2008) Hologram optimization for slm-based reconstruction with regard to polarization effects. *Opt. Express*, **16** (19), 14853–14861. doi: 10.1364/OE.16.014853.

41. Kohler, C., Haist, T., and Osten, W. (2009) Model-free method for measuring the full Jones matrix of reflective liquid-crystal displays. *Opt. Eng.*, **48** (4), 044002. doi: 10.1117/1.3119309.

42. Meeser, T., von Kopylow, C., and Falldorf, C. (2010) Advanced digital lensless Fourier holography by means of a spatial light modulator. 3DTV-Conference: The True Vision - Capture, Transmission and Display of 3D Video (3DTV-CON), 2010, pp. 1–4, 79.

43. Falldorf, C., Klattenhoff, R., and Gesierich, A. (2009) Lateral shearing interferometer based on a spatial light modulator in the Fourier plane, in *Fringe 2009: 6th International Workshop on Advanced Optical Metrology* (eds W., Osten and M. Kujawinska), Springer Heidelberg, pp. 93–98.

44. Schaal, F., Warber, M., Rembe, C., Haist, T., and Osten, W. (2009) Dynamic multipoint vibrometry using spatial light modulators, in *Fringe 2009, 6th International Workshop on Advanced Optical Metrology* (eds M. Osten and W. Kujawinska), Springer, pp. 528–531.

45. Baumbach, T., Osten, W., von Kopylow, C., and Jüptner, W. (2006) Remote metrology by comparative digital holography. *Appl. Opt.*, **45** (5), 925–934. doi: 10.1364/AO.45.000925.

46. Jenness, N.J. (2009) Three-dimensional holographic lithography and manipulation using a spatial light modulator. PhD thesis. Duke University.

47. Jenness, N.J., Wulff, K.D., Johannes, M.S., Padgett, M.J., Cole, D.G., and Clark, R.L. (2008) Three-dimensional parallel holographic micropatterning using a spatial light modulator. *Opt. Express*, **16** (20), 15942–15948. doi: 10.1364/OE.16.015942.

48. Jenness, N.J., Hill, R.T., Hucknall, A., Chilkoti, A., and Clark, R.L. (2010) A versatile diffractive maskless lithography for single-shot and serial microfabrication. *Opt. Express*, **18** (11), 11754–11762. doi: 10.1364/OE.18.011754.

49. Li, J., Wen, C.-H., Gauza, S., Lu, R., and Wu, S.-T. (2005) Refractive indices of liquid crystals for display applications. *J. Display Technol.*, **1** (1), 51.

50. Gauza, S., Wen, C.-H., Tan, B., and Wu, S.-T. (2004) UV stable high birefringence liquid crystals. *Jpn. J. Appl. Phys.*, **43**, 7176–+. doi: 10.1143/JJAP.43.7176.

51. von Freymann, G., Ledermann, A., Thiel, M., Staude, I., Essig, S., Busch, K., and Wegener, M. (2010) Three-dimensional nanostructures for photonics. *Adv. Funct. Mater.*, **20** (7), 1038–1052. ISSN 1616-3028. doi: 10.1002/adfm.200901838.

52. Nikolenko, V., Watson, B.O., Araya, R., Woodruff, A., Peterka, D.S., and Yuste, R. (2008) SLM microscopy: scanless two-photon imaging and photostimulation with spatial light modulators. *Front Neural Circuits*, **2** (5), 1–14.

53. Fratz, M., Fischer, P., and Giel, D.M. (2009) Full phase and amplitude control in computer-generated holography. *Opt. Lett.*, **34** (23), 3659–3661. doi: 10.1364/OL.34.003659.

54. Kuang, Z., Perrie, W., Liu, D., Edwardson, S., Cheng, J., Dearden, G., and Watkins, K. (2009) Diffractive multi-beam surface micro-processing using 10 ps laser pulses. *Appl. Surf. Sci.*, **255** (22), 9040–9044. ISSN 0169-4332. doi: 10.1016/j.apsusc.2009.06.089.

55. Hermerschmidt, A., Krüger, S., Haist, T., Zwick, S., Warber, M., and Osten, W. (2007c) Holographic optical tweezers with real-time hologram calculation using a phase-only modulating LCOS-based SLM at 1064 nm. *SPIE Proc.*, **6905**,. doi: 10.1117/12.764649.

56. Hirvonen, L., Wicker, K., Mandula, O., and Heintzmann, R. (2009) Structured illumination microscopy of a living cell. *Eur. Biophys. J.*, **38**,

807–812. ISSN 0175-7571. doi: 10.1007/s00249-009-0501-6.

57. Chang, B.-J., Chou, L.-J., Chang, Y.-C., and Chiang, S.-Y. (2009) Isotropic image in structured illumination microscopy patterned with a spatial light modulator. *Opt. Express*, **17**, 14710–+. doi: 10.1364/OE.17.014710.

58. Heintzmann, R. (2003) Saturated patterned excitation microscopy with two-dimensional excitation patterns. *Micron*, **34** (9), 283–291. doi: 10.1016/S0968-4328(03)00053-2.

59. Hayasaki, Y., Sumi, S., Mutoh, K., Suzuki, S., Itoh, M., Yatagai, T., and Nishida, N. (1996) Optical manipulation of microparticles using diffractive optical elements, in *SPIE Proceedings*, vol. **2778**, (eds J.-S. Chang, J.-H. Lee, S.-Y. Lee, and C.H. Nam), SPIE, pp. 229–+.

60. Dufresne, E.R. and Grier, D.G. (1998) Optical tweezer arrays and optical substrates created with diffractive optics. *Rev. Sci. Instrum.*, **69**, 1974–1977. doi: 10.1063/1.1148883.

61. Reicherter, M., Haist, T., Wagemann, E.U., and Tiziani, H.J. (1999) Optical particle trapping with computer-generated holograms written on a liquid-crystal display. *Opt. Lett.*, **24** (9), 608–610. doi: 10.1364/OL.24.000608.

62. Haist, T., Zwick, S., Warber, M., and Osten, W. (2006) Spatial light modulators - versatile tools for holography. *J. Hologr. Speckle*, **3** (12), 125–136. doi: doi:10.1166/jhs.2006.019.

63. Zwick, S., Warber, M., Gorski, W., Haist, T., and Osten, W. (2009) Flexible adaptive phase contrast methods using a spatial light modulator. Proceedings DGAO, vol. A3.

64. Situ, G., Warber, M., Pedrini, G., and Osten, W. (2010) Phase contrast enhancement in microscopy using spiral phase filtering. *Opt. Commun.*, **283** (7), 1273–1277. ISSN 0030-4018. doi: 10.1016/j.optcom.2009.11.084.

65. Warber, M., Zwick, S., Hasler, M., Haist, T., and Osten, W. (2009) SLM-based phase-contrast filtering for single and multiple image acquisition, in *SPIE Proceedings*,

Optics and Photonics for Information Processing III, vol. **7442**, (K.M. Iftekharuddin and A.A.S. Awwal), SPIE. doi: 10.1117/12.825945.

66. Takeda, M., Wang, W., and Nai, D.N. (2009) Coherence holography: a thought on synthesis and analysis of optical coherence fields, in *Fringe 2009, 6th International Workshop on Advanced Optical Metrology* (eds M. Osten and W. Kujawinska), Springer, pp. 14–+.

67. Rosen, J. and Brooker, G. (2008) Non-scanning motionless fluorescence three-dimensional holographic microscopy. *Nat. Photonics*, **2**, 190–195. doi: 10.1038/nphoton.2007.300.

68. Brooker, G., Siegel, N., Wang, V., and Rosen, J. (2011) Optimal resolution in Fresnel incoherent correlation holographic fluorescence microscopy. *Opt. Express*, **19**, 5047–+. doi: 10.1364/OE.19.005047.

69. Katz, B. and Rosen, J. (2011) Could SAFE concept be applied for designing a new synthetic aperture telescope? *Opt. Express*, **19**, 4924–+. doi: 10.1364/OE.19.004924.

70. Maurer, C., Jesacher, A., Bernet, S., and Ritsch-Marte, M. (2011) What spatial light modulators can do for optical microscopy. *Laser & Photonics Rev.*, **5** (1), 81–101. ISSN 1863-8899. doi: 10.1002/lpor.200900047.

71. Auksorius, E. (2008) Multidimensional fluorescence imaging and super-resolution exploiting ultrafast laser and supercontinuum technology. PhD thesis. Imperial College London.

72. Auksorius, E., Boruah, B.R., Dunsby, C., Lanigan, P.M.P., Kennedy, G., Neil, M.A.A., and French, P.M.W. (2008) Stimulated emission depletion microscopy with a supercontinuum source and fluorescence lifetime imaging. *Opt. Lett.*, **33** (2), 113–115. doi: 10.1364/OL.33.000113.

73. Mudry, E., Le Moal, E., Ferrand, P., Chaumet, P.C., and Sentenac, A. (2010) Isotropic diffraction-limited focusing using a single objective lens. *Phys. Rev. Lett.*, **105** (20), 203903–+. doi: 10.1103/PhysRevLett.105.203903.

74. Beversluis, M.R., Novotny, L., and Stranick, S.J. (2006) Programmable vector point-spread function engineering. *Opt. Express*, **14** (7), 2650–2656. doi: 10.1364/OE.14.002650.

75. Chen, H., Zheng, Z., Zhang, B.-F., Ding, J., and Wang, H.-T. (2010) Polarization structuring of focused field through polarization-only modulation of incident beam. *Opt. Lett.*, **35** (16), 2825–2827. doi: 10.1364/OL.35.002825.

76. Wang, X.-L., Ding, J., Ni, W.-J., Guo, C.-S., and Wang, H.-T. (2007) Generation of arbitrary vector beams with a spatial light modulator and a common path interferometric arrangement. *Opt. Lett.*, **32** (24), 3549–3551. doi: 10.1364/OL.32.003549.

77. Chen, W. and Zhan, Q. (2010) Diffraction limited focusing with controllable arbitrary three-dimensional polarization. *J. Opt.*, **12** (4), 045707.

78. Dorn, R., Quabis, S., and Leuchs, G. (2003) Sharper focus for a radially polarized light beam. *Phys. Rev. Lett.*, **91** (23), 233901−+. doi: 10.1103/PhysRevLett.91.233901.

79. Chen, W. (2009) Focus engineering with spatially variant polarization for nanometer scale applications. PhD thesis. The School of Engineering of the University of Dayton.

80. Wang, H., Shi, L., Lukyanchuk, B., Sheppard, C., and Chong, C.T. (2008) Creation of a needle of longitudinally polarized light in vacuum using binary optics. *Nat. Photonics*, **2**, 501–505. doi: 10.1038/nphoton.2008.127.

81. Bashkansky, M., Park, D., and Fatemi, F.K. (2010) Azimuthally and radially polarized light with a nematic SLM. *Opt. Express*, **18** (1), 212–217. doi: 10.1364/OE.18.000212.

82. Beversluis, M.R. and Stranick, S.J. (2008) Enhanced contrast coherent anti-Stokes Raman scattering microscopy using annular phase masks. *Appl. Phys. Lett.*, **93** (23), 231115−+. doi: 10.1063/1.3046719.

83. Zhan, Q. (2009) Cylindrical vector beams: from mathematical concepts to applications. *Adv. Opt. Photon.*, **1** (1), 1–57. doi: 10.1364/AOP.1.000001.

84. Frumker, E. and Silberberg, Y. (2007) Phase and amplitude pulse shaping with two-dimensional phase-only spatial light modulators. *J. Opt. Soc. Am. B*, **24** (12), 2940–2947. doi: 10.1364/JOSAB.24.002940.

85. Kali, A., Tan, A., Gravey, P., Wolffer, N., Lelah, A., and Pincemin, E. (2003) Assessment of LCOS technology for the realization of scalable $n \times n$ optical switches. Proceedings of International Conference on Photonics in Switching (PS 2003).

86. Roelens, M.A., Bolger, J.A., Williams, D., and Eggleton, B.J. (2008) Multi-wavelength synchronous pulse burst generation with a wavelength selective switch. *Opt. Express*, **16** (14), 10152–10157. doi: 10.1364/OE.16.010152.

87. Frisken, S.J. (2009) Optical communications system. US Patent 7593608.

88. Leister, N., Schwerdtner, A., Fütterer, G., Buschbeck, S., Olaya, J.-C., and Flon, S. (2008) Full-color interactive holographic projection system for large 3D scene reconstruction. *SPIE Proc.*, **6911**,. doi: 10.1117/12.761713.

89. Onural, L., Yaras, F., and Kang, H. (2010) Digital holographic three-dimensional video displays. *Proc. IEEE*, **99**,. doi: 10.1109/JPROC.2010.2098430.

90. Buckley, E. (2008) Holographic laser projection technology. *SID Symp. Dig. Tech. Pap.*, **39** (1), 1074–1079. doi: 10.1889/1.3069321.

91. Liang, J., Williams, D.R., and Miller, D.T. (1997) Supernormal vision and high-resolution retinal imaging through adaptive optics. *J. Opt. Soc. Am. A*, **14** (11), 2884–2892. doi: 10.1364/JOSAA.14.002884.

92. Hendricks, U., Krüger, S., Brandt, P., Charle, H., and Sahlbom, D. (2008) Holographic information display. US Patent Application 2008/0192312 A1.

93. Goodman, J.W. (1976) Some fundamental properties of speckle. *J. Opt. Soc. Am.*, **66** (11), 1145–1150. doi: 10.1364/JOSA.66.001145.

94. Marchese, L., Bourqui, P., Turgeon, S., Doucet, M., Vachon, C., Harnisch, B., Suess, M., Châteauneuf,

F., and Bergeron, A. (2010) A SAR multilook optronic processor for operational Earth monitoring applications, in *SPIE Proceedings*, SAR Image Analysis, Modeling, and Techniques X, vol. **7829**, (ed. C. Notarnicola), pp. 782904. doi: 10.1117/12.866986.

95. Vellekoop, I.M. and Mosk, A.P. (2007) Focusing coherent light through opaque strongly scattering media. *Opt. Lett.*, **32** (16), 2309–2311.

96. Becker, C., Stellmer, S., Soltan-Panahi, P., Dörscher, S., Baumert, M., Richter, E.-M., Kronjäger, J., Bongs, K., and Sengstock, K. (2008) Oscillations and interactions of dark and dark bright solitons in Bose Einstein condensates. *Nat. Phys.*, **4**, 496–501. doi: 10.1038/nphys962.

97. Boyer, V., Godun, R.M., Smirne, G., Cassettari, D., Chandrashekar, C.M., Deb, A.B., Laczik, Z.J., and Foot, C.J. (2006) Dynamic manipulation of Bose–Einstein condensates with a spatial light modulator. *Phys. Rev. A*, **73** (3), 031402−+. doi: 10.1103/PhysRevA.73.031402.

98. Bromberg, Y., Katz, O., and Silberberg, Y. (2009) Ghost imaging with a single detector. *Phys. Rev. A*, **79** (5), 053840. doi: 10.1103/PhysRevA.79.053840.

99. Stütz, M., Gröblacher, S., Jennewein, T., and Zeilinger, A. (2007) How to create and detect n-dimensional entangled photons with an active phase hologram. *Appl. Phys. Lett.*, **90** (26), 261114. doi: 10.1063/1.2752728.

100. Lima, G., Vargas, A., Neves, L., Guzmán, R., and Saavedra, C. (2009) Manipulating spatial qudit states with programmable optical devices. *Opt. Express*, **17** (13), 10688–10696. doi: 10.1364/OE.17.010688.